Interaction of water with PuO_2 analogues

D. M. Laventine[1]*, C. Boxall[1], R. Taylor[2] and R. Orr[2]

[1] Department of Engineering, University of Lancaster, Lancaster, LA1 4YR, UK.
[2] Central laboratory, B170, National Nuclear Laboratory, Sellafield, CA20 1PG, UK
* d.laventine@lancaster.ac.uk

Introduction

Approximately 250 tonnes of separated Pu are currently stockpiled worldwide. ~50% is in interim storage in the UK whilst further processing or long-term storage options are considered.

Interim storage of PuO_2 involves sealing in inert steel containers under a partially inert atmosphere. Under certain circumstances, these gas canisters have been observed to spontaneously heat up and pressurise. A number of routes of gas production have been postulated to explain the increase in pressure, including the thermal desorption of water from the hygroscopic PuO_2 and the radiolysis of adsorbed water. The aim of this project is to investigate the interaction of plutonium oxide (and less radioactive analogues) with water using contact angle measurements and crystal nano-balance methodologies

Fig. 1. Interim storage canister of PuO_2 powder.

Thin Film Synthesis

Substrates (Pt, glass) have been coated with metal oxide (PuO_2, CeO_2, ThO_2, U_3O_8) thin-films by drop-coating with solutions of $M(NO_3)_3$ in nitric acid and methanol. Calcination at 300-500°C under air produced MO_2 layers of 40–1000 nm thick that were analysed by SEM (fig. 1) and Raman spectroscopy

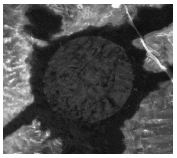

Fig. 2. SEM of PuO_2-coating (on Pt & borosilicate glass, 450°C calcine).

Contact Angle Measurement

Sessile water droplets (1-10 µm) were deposited onto oxide coated thin films, and their dimensions measured using a backlit light microscope in a sealed container. Initial humidity was controlled by evaporation of added water, and temperature and humidity monitored. Initial contact angles (I.C.A) were measured, and changes to the droplet dimensions (droplet radius, height) monitored until complete evaporation of the droplet was observed. Computer vision algorithms were used to automate measurements, and the contact angles calculated by modelling as hemispheroidal slices of constructed spheres (fig. 5).

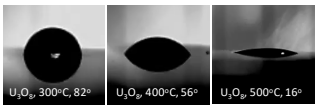

Fig. 3 Droplets on U_3O_8 thin-films calcined at different temperatures, showing decrease in I.C.A.

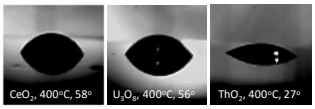

Fig. 4. Droplets on different metal oxide layers calcined at same temperature.

Pilot experiments have shown the calcination temperature used in the synthesis of the oxide layers was found to have a large effect on initial contact angle (fig. 3), with higher calcination temperatures resulting in more hydrophilic surfaces (lower I.C.A). The contact angle also depended upon the metal species of the coating, showing significant differences in wettability of the surfaces (fig. 4). More hydrophilic surfaces showed larger stick-shift events during evaporation, in which droplet radius remained static while the height decreased, followed by abrupt contractions of the droplet, increasing the observed contact angle (fig. 6).

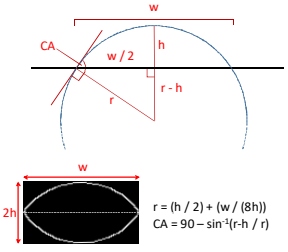

Fig. 5. Contour mask of water droplet, with geometry of contact angle calculation

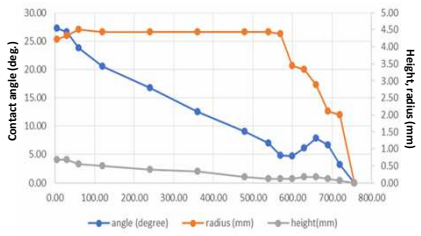

Fig. 6. Dimensions of 1 µm droplet during evaporation from ThO_2 thin-film (calcined at 400°C, humidity 40%, I.C.A= 27°

Piezo-crystal Nano-balance

Crystal microbalances utilise the piezoelectric effect to accurately measure very small changes in mass of a crystal, via changes in the frequency of the crystal vibration in response to an applied current. Through coating the crystal with a thin layer of the metal oxide of interest, any changes in frequency due to absorption or desorption of gases at the oxide surface can be measured, and the change in mass determined using the Sauerbrey equation.

$$\Delta f = -\left(\frac{n{f_0}^2}{A\sqrt{\rho_q \mu_q}}\right)\Delta m$$

Eqn. 2. Sauerbrey equation

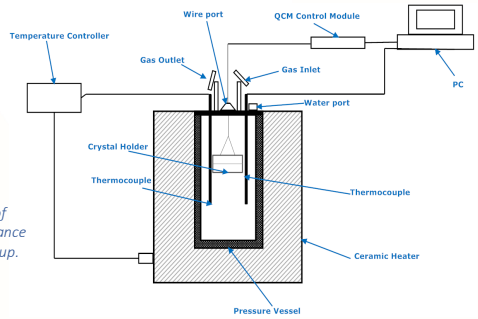

Fig. 7. Diagram of crystal nano-balance experimental setup.

The resonant frequency of the coated crystals was then measured in a sealed reaction vessel in the presence of water, which showed that an increase in mass occurred as water was absorbed onto the metal oxide layers in a manner consistent with type II/IV absorption isotherms (fig. 8).

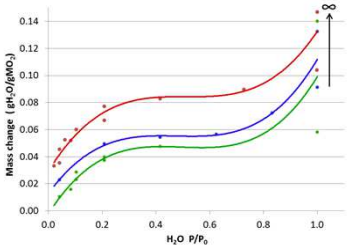

Fig. 8. Mass change due to water adsorption on 40-60 nm thick MO_x coated $GaPO_4$ crystals at 75°C.

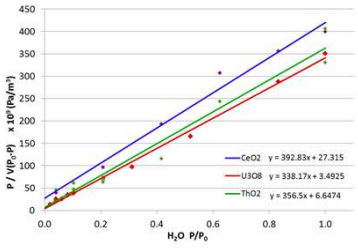

Fig. 9. BET plot of water adsorbed on 40-60 nm thick MO_x coated $GaPO_4$ crystals at 75°C.

Application of the BET equation afforded straight line plots (fig. 9), allowing the calculation of the enthalpy of absorption of water and the surface area of the samples.

The temperature of systems at initial saturated vapour pressure (at 75°C) was then varied up to 375°C, showing that the absorbed water is desorbed as the sample is heated and the partial pressure of water in the atmosphere is reduced (fig. 10).

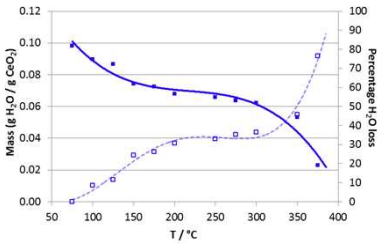

Fig. 10. Water desorption from 40 nm thick CeO_2-coated $GaPO_4$ crystals from 75°C (at sat. VP) to 375°C.

Conclusions and Further work

Ceria, thoria, and uranium oxide nanoscale layers have been produced on glass and piezo-crystal electrode surfaces. Contact angle measurements showed the wettability of the surfaces to be vary by the metal oxide used, and due to the calcination temperature used.

The absorption of water across a range of partial pressures of water has been investigated by piezoelectric nano-balance, leading to estimated for the enthalpy of binding of water to the surface of the oxides. Increasing the temperature of the system to mimic real-world storage conditions has show that significant amounts of water are still present on the oxide surface even up to 400ºC, indicating that nuclear waste-forms will contain appreciable amounts of water even after heat treatment. Work is ongoing to transfer these experimental setups to Central Laboratory of the National Nuclear Laboratory, allowing wettability and water absorption properties of PuO_2 itself.

Acknowledgements: This work was funded by the EPSRC as part of the Transcend consortium and further supported by the European ActusLab framework and the Lloyd's Register Foundation (LRF), a UK registered charity.

The Defect Chemistry of PuO_2

William Neilson*, Dr. Samuel T. Murphy

Department of Engineering, Lancaster University, Lancaster, LA1 4YR

*w.neilson@lancaster.ac.uk

Introduction

The handling, storage and disposal of PuO_2 presents considerable safety and security challenges, necessitating investigation of the material.

PuO_{2+x} phases are reported to participate in moisture enhanced corrosion of the plutonium metal, producing hydrogen which could potentially result in formation of explosive gases and generation of pressures that cause loss of containment and dispersal of Pu-containing particles.

Studying the defect chemistry of PuO_2 aids description of the formation and properties of non-stoichiometric PuO_2, as well as relationship with temperature and oxygen partial pressure.

Methods

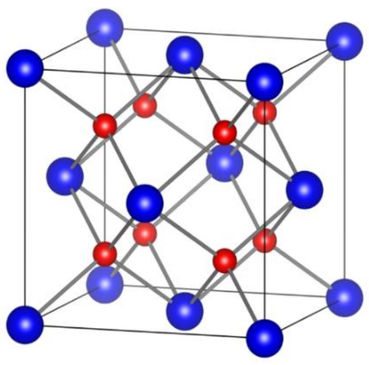

$Fm\bar{3}m$ crystal symmetry
12 atoms
Pu (blue)
O (red)

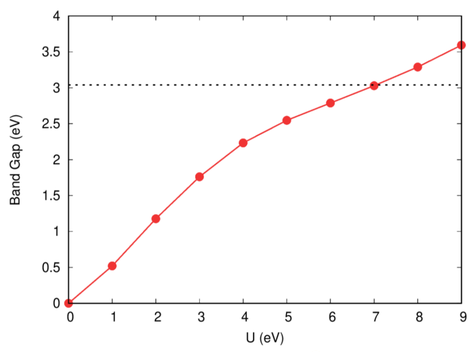

← BAND GAP TARGET

Computational method:
VASP, PBEsol + U
U = 7.0 eV, reproducing hybrId functional (HSE06) band gap (3.04 eV)

ADD OXYGEN ATOMS

Oxygen interstitials: $O_i^{\times}$, O_i^{1-} and O_i^{2-}

REMOVE OXYGEN ATOMS

Oxygen vacancies: $V_O^{\times}$, V_O^{1+} and V_O^{2+}

ADD PLUTONIUM ATOMS

Plutonium interstitials: $Pu_i^{\times}$, Pu_i^{1+}, Pu_i^{2+}, Pu_i^{3+} and Pu_i^{4+}

REMOVE PLUTONIUM ATOMS

Plutonium vacancies: $V_{Pu}^{\times}$, V_{Pu}^{1-}, V_{Pu}^{2-}, V_{Pu}^{3-} and V_{Pu}^{4-}

Start with PuO_2 unit cell → Apply magnetic properties → Simulate using Density Functional Theory (DFT) → Create PuO_2 supercell → Add defects to supercell & re-simulate to obtain defect energies → Calculate formation energy of each defect, as a function of Fermi level

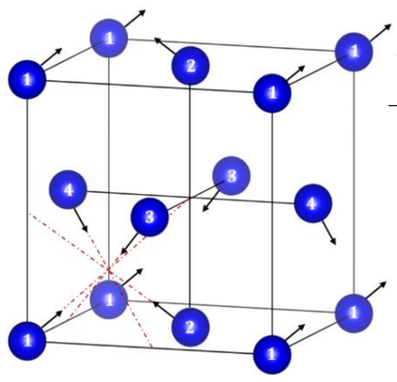

Atom	Magnetic moment
1	(1, 1, 1)
2	(-1, -1, 1)
3	(-1, 1, -1)
4	(1, -1, -1)

Longitudinal 3k anti-ferromagentic ground-state found and adopted

2 x 2 x 2, 96 atoms

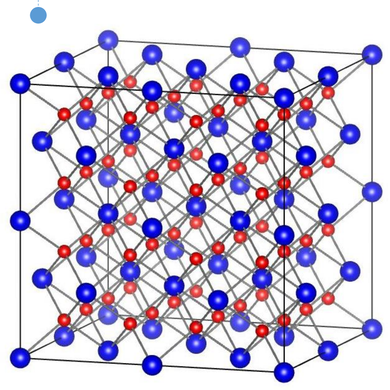

Change in vibrational entropy, ΔS_{vib}, due to defect incorporation is included in formation energy.

V_O
O_i
V_{Pu}
Pu_i

CHARGE STATE WITH LOWEST FORMATION ENERGY PLOTTED

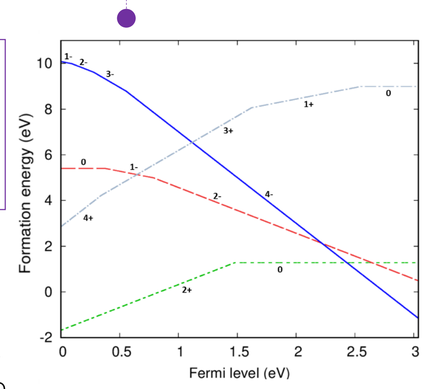

Results

BROUWER DIAGRAM - DEFECT CONCENTRATION, OXYGEN PARTIAL PRESSURE DEPENDENCE
TEMPERATURE: 1000 K

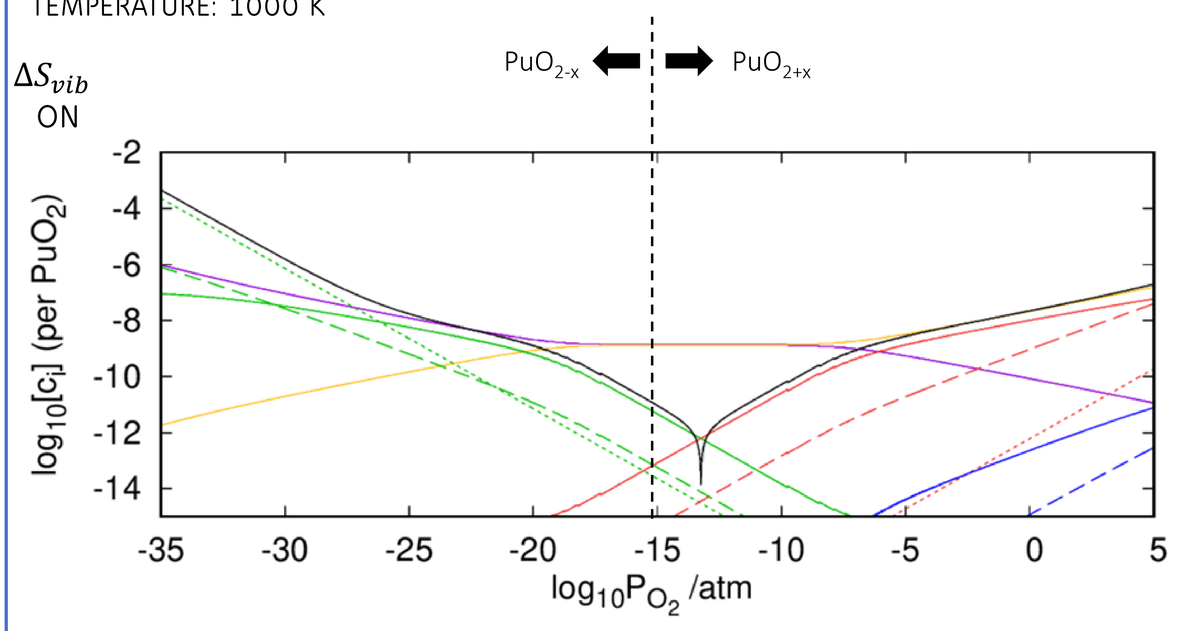

DEFECT CONCENTRATION, TEMPERATURE DEPENDENCE
OXYGEN PARTIAL PRESSURE: 10^{-2} atm

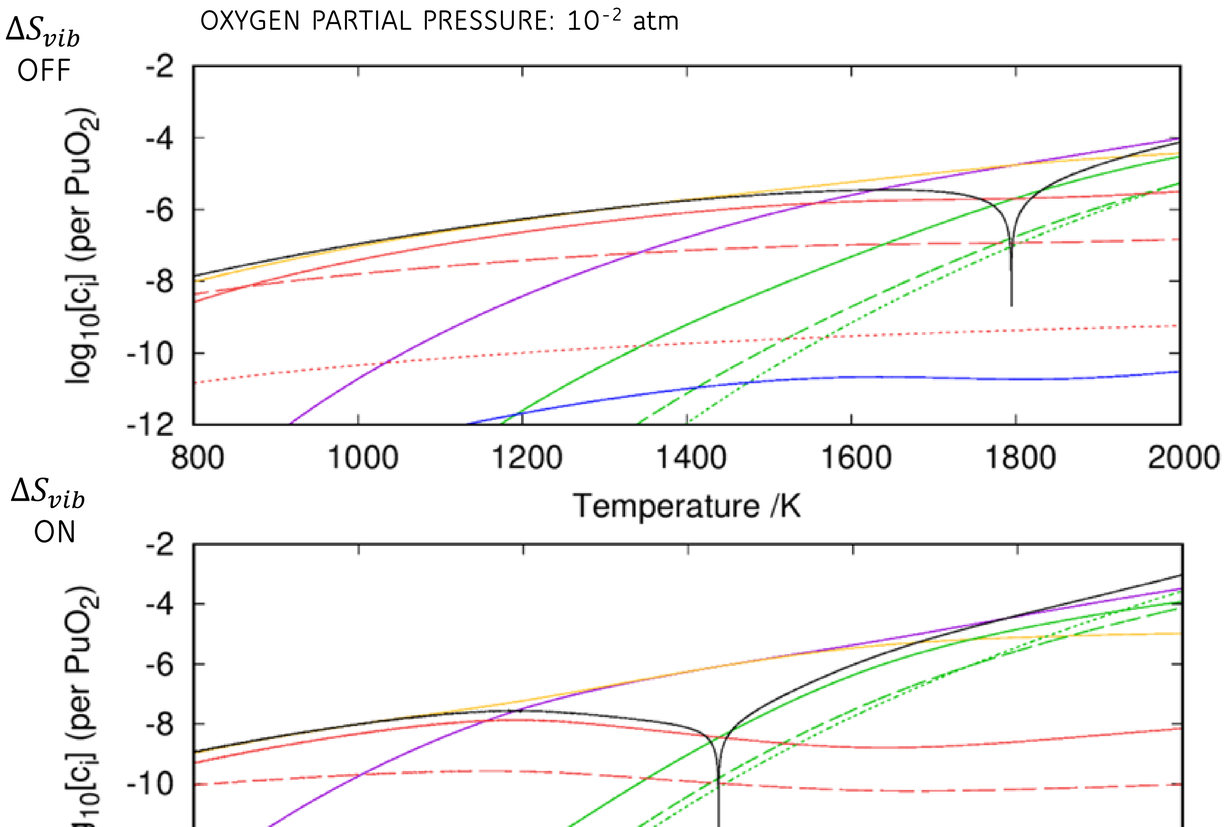

Conclusions

- Oxygen defects dominant.
- Hyper-stoichiometry negligible.
- Formally charged defects dominate at near-stoichiometry, non-formally charged defects become dominant with increased non-stoichiometry.
- Vibrational entropy contributes significantly.

Acknowledgements

I thank J.T. Pegg, D.O. Scanlon and M. Pacey for their valuable help. This work made use of the High End Computing facility at Lancaster University. The visualisation of crystal structures was performed with VESTA, finite-size corrections were calculated using pymatgen.

Lancaster University

Transformative Science and Engineering for Nuclear Decommissioning

EPSRC Engineering and Physical Sciences Research Council | UK Research and Innovation

transcendconsortium.org

Energy For a Low Carbon Future

Energy landscape of water dissociation on ThO_2(111) surface

Xiaoyu Han, Nikolas Kaltsoyannis

Department of Chemistry, University of Manchester, Oxford Road, Manchester, M13 9PL

nikolas.kaltsoyannis@manchester.ac.uk

Introduction

Here we investigated the water reaction on ThO_2 (111) surface using Density Functional Theory (DFT). Prior to the water reaction, we have benchmarked the parameter settings for bulk ThO_2 on functionals, LSDA+U approaches. Through the study on water adsorption, dissociation and interaction with another single water molecule, H* radical, and H^+ ion, we could give the full spectrum of free energy landscape of water dissociation on the ThO_2 (111) surface.

Computation details

All the calculations were carried out based on Density Functional Theory (DFT), which implanted in the Vienna ab-initio Package (VASP).[1] The Projector Augmented Wave (PAW) methods used to treat the core electrons, with the plane wave cutoff set to 650 eV.[2] Both PBE and LDA functional were adopted to evaluate its prediction on lattice parameters and bandgap.[3,4] Geometry relaxation and vibrational frequency calculation used Gaussian electronic smearing. And the final energy was obtained with tetrahedron method with Blöchl corrections until the energy difference was less than 10^{-5} eV. In order to describe this strongly correlated systems, two LSDA+U scheme (Dudarev approach[5] and Liechtenstein approach[6]) and hybrid functionals were compared.

For bulk calculations, the Brillouin zone was sampled using a 5x5x5 and a 25x25x25 kpoint mesh for geometry optimisation and Projected Density of States (PDOS), respectively. For the surface calculations, the (111) surface was built by 2*2 supercell with 5 layers. The bottom 2 layers keep fixed while all other atoms are fully relaxed. Each slab was inserted 15 Å vacuum slab to prevent periodic interactions. Dipole-field corrections was considered to remove spurious interaction between periodic images perpendicular to the surfaces. The Brillouin zone was sampled using a 5*5*1 mesh with Gamma centred for the slab. The van der Waals correction was adopted the DFT-D4 method.[7]

The free energy of each reaction was calculated based on $\Delta G = \Delta E + \Delta ZPE - T\Delta S$, where ΔE is the adsorption energy. It could be calculated $\Delta E = \Delta E_{total} - \Delta E_{sub} - \Delta E_{adsorbant}$. The ΔZPE is the changes of zero-point energy and ΔS is the entropy difference, which were taken from the reference database[8]. The transition states were determined by the Climbing-Image Nudged Elastic Band.[9] The rate constant is based on the Arrhenius theory and Transition state theory, $k = \frac{k_B T}{h} e^{-\frac{\Delta G}{RT}} = \frac{k_B T}{h} e^{\frac{\Delta S}{R}} e^{-\frac{\Delta H}{RT}}$

Results

0. Bulk ThO_2

To fully mimic the ThO_2, both the lattice parameter and bandgap were taken as the criteria to evaluate the computational settings. Here we adopt the root mean square error (σ_{RMS}) of each parameter to evaluate its performance on both lattice parameter and band gap, i.e. $\sigma_{RMS} = \sqrt{\frac{(\sigma_L^2 + \sigma_{gap}^2)}{2}}$, where $\sigma_L = \frac{L - L_{exp.}}{L_{exp.}}$ and $\sigma_{gap} = \frac{\Delta G - \Delta G_{exp.}}{\Delta G_{exp.}}$.

0.1 The Dudarev approach $E_{DFT+U} = E_{DFT} + \frac{U-J}{2}\sum_{m\sigma}(n_{m\sigma} - n_{m\sigma}^2)$

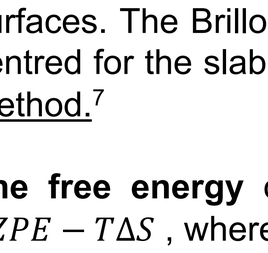

1) GGA functional performs better overall.
2) Spin-orbital coupling is not significant in ThO_2
3) U_{eff}=5 better than U_{eff}=4

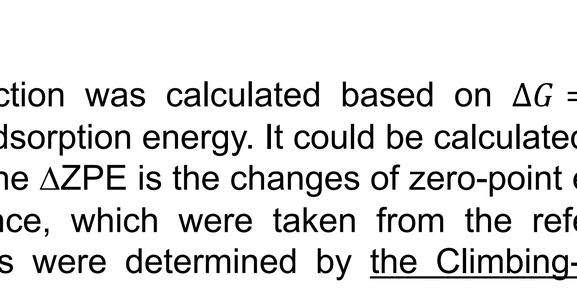

0.2 The Liechtenstein approach

$$E_{LDA+U} = E_{DFT} + E_{HF} - E_{dc}(\hat{n})$$
$$E_{dc}(\hat{n}) = \frac{U}{2}\hat{n}_{total}(\hat{n}_{total} - 1) - \frac{J}{2}\sum_{\sigma}\hat{n}_{tot}^{\sigma}(\hat{n}_{tot}^{\sigma} - 1)$$

1) The Liechtenstein approach improve the electronic interaction on the non-diagonal part in the matrix.
2) The optimized parameters are U=7, J=1 with GGA.

1. H_2O on ThO_2 (111) --- step 0

$H_2O + * \rightarrow {}^{*}_{0,2}H_2O$

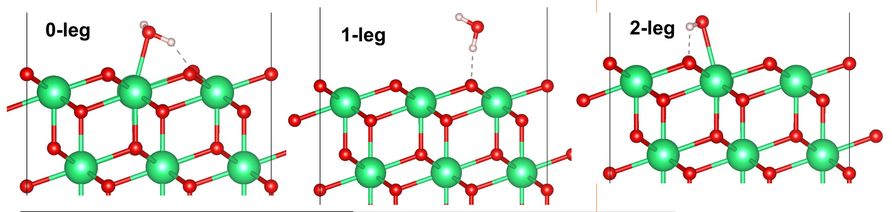

the lone pair > the H bonds

ΔG_0	298K (RT)	500K
0-leg	-0.82 eV	-1.31 eV
1-leg	-0.46 eV	-0.95 eV
2-leg	-0.78 eV	-1.26 eV

- **Exothermic reaction**
- **High T promotes the reaction**

2. H_2O dissociation --- step 1

${}^{*}_{0}H_2O \rightarrow {}^{*}_{0}OH + {}^{*}_{0}H$

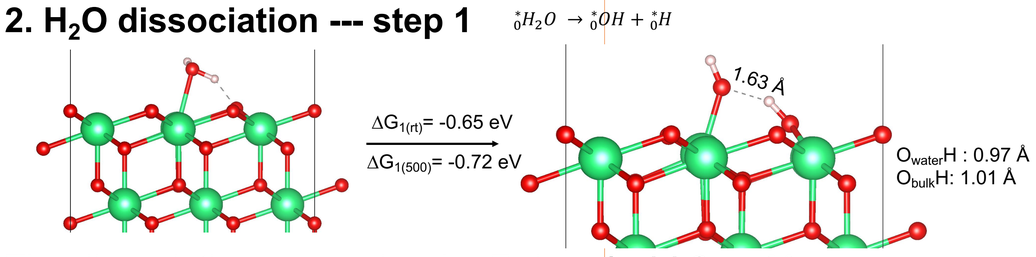

The dissociation energy barrier E_d is only **14.8 meV.**

3.1.1 2nd water adsorption

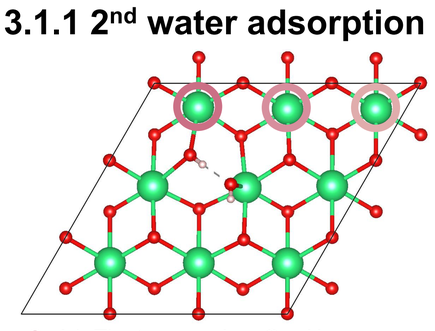

- A1: Th atom nearby $-O_{bulk}H$ group
- A2: Th atom nearby $-O_{water}H$ group
- A3: far away

	A1	A2	A3
E_{ad}	-1.06 eV	-0.89 eV	-0.86 eV
$\Delta G_{2(rt)}$	-0.89 eV	-0.77eV	-0.72 eV
$\Delta G_{2(500)}$	-1.38 eV	-1.26 eV	-1.21 eV

$O_{bulk}H$ group **promotes the 2nd water adsorption**

3.1.2 2nd water dissociation

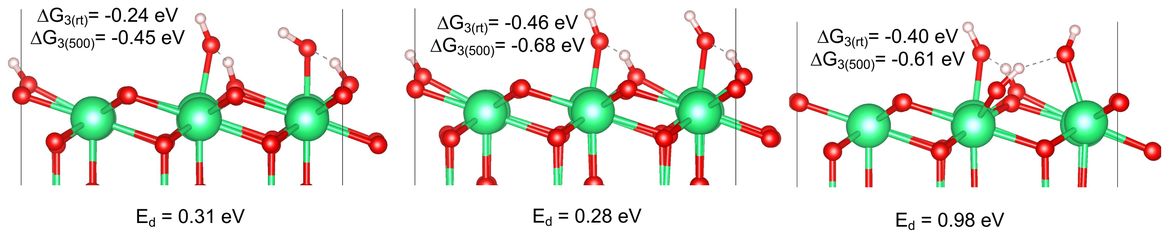

- Compared with 1st water adsorption, the 2nd water is much harder;
- High reaction energy barrier indicates the 2nd water in the far away from the 1st water can't dissociate.

3.2.1 & 3.2.2 H^+ ion and H* radical at pH=7

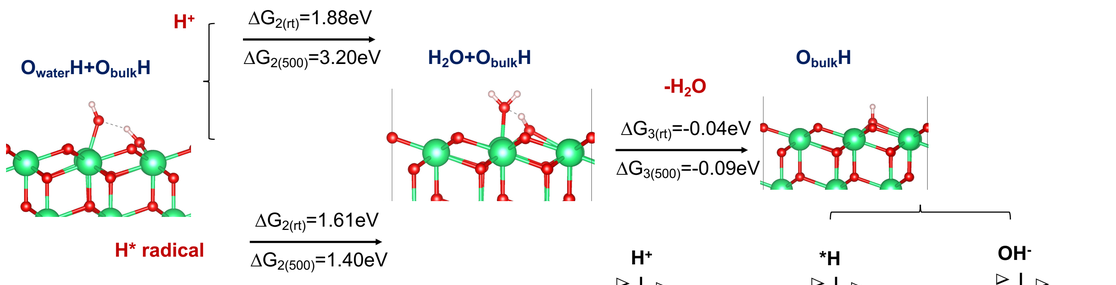

- It is hard for dissociated water interacts with H^+ and H* radical.
- Protonated surface could prevent water adsorption. However, it is also easy to generate H_2 with H^+ or H* radical.

Conclusion

- The Liechtenstein approach LSDA+U method improves on both lattice parameter and bandgap of ThO_2;
- For (111) surface, the lone pair electron of water outperforms the hydrogen bond;
- It's an exothermic reaction for water adsorbs and could be further dissociated at RT;
- The dissociated water promotes the 2nd water adsorption. The binding energy is even stronger than the 1st one;
- The 2nd water dissociation only could happen in the nearby position with ~0.3 eV energy barrier;
- Protonated surface could prevent the water adsorption. However, it also offers the generation of H_2 gas.

Acknowledgement

We would like to acknowledge the financial support from **EP/S01019X/1** and useful discussion with the **Transcend** consortium. We also would like to acknowledge the used of the Archer High performance computing facility, and associated support services, in the completion of the simulation work.

Gas Generation from the radiolysis of water on Uranium oxides and ThO_2

Christopher Anderson, Mel O'Leary, , Frederick Currell
Dalton Cumbria Facility, The University of Manchester
christopher.anderson-3@postgrad.manchester.ac.uk

Project Overview

The radiolysis of water produces several stable and unstable products including H_2 which creates potentially challenging situations for the safe storage of PuO_2. Introducing an oxide/water interface significantly impacts H_2 yield and as such, ThO_2, UO_2, UO_3, and U_3O_8 powders have been selected as suitable surrogate materials to simulate radiolytic processes for PuO_2 in storage. These were selected due to them being low α-emitters and in some cases, sharing a similar crystalline structure. Before experiments can be conducted, a new manifold must be developed.

Industrial Context

- The United Kingdom has approximately 140 tonnes of stockpiled Plutonium as PuO_2 powder in interim storage at the Sellafield site.
- A re-use strategy could take 15 years to implement, thus the powder will have to remain in storage for the foreseeable future.
- Some powder has already been in storage for decades raising concerns regarding container longevity, especially if pressurisation occurs due to radiolytically produced gas.

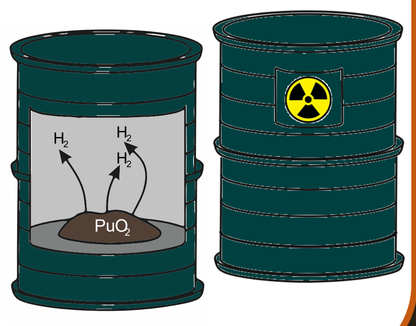

Experimental Apparatus Design

The new manifold has been designed and developed to include the following:

- Modular and easily re-configurable components to suit a wide range of purposes and experiments.
- Increased automation to allow in-situ changes and monitoring.
- Several slots for repeating sample units so several experiments can run concurrently.
- More control over external influences

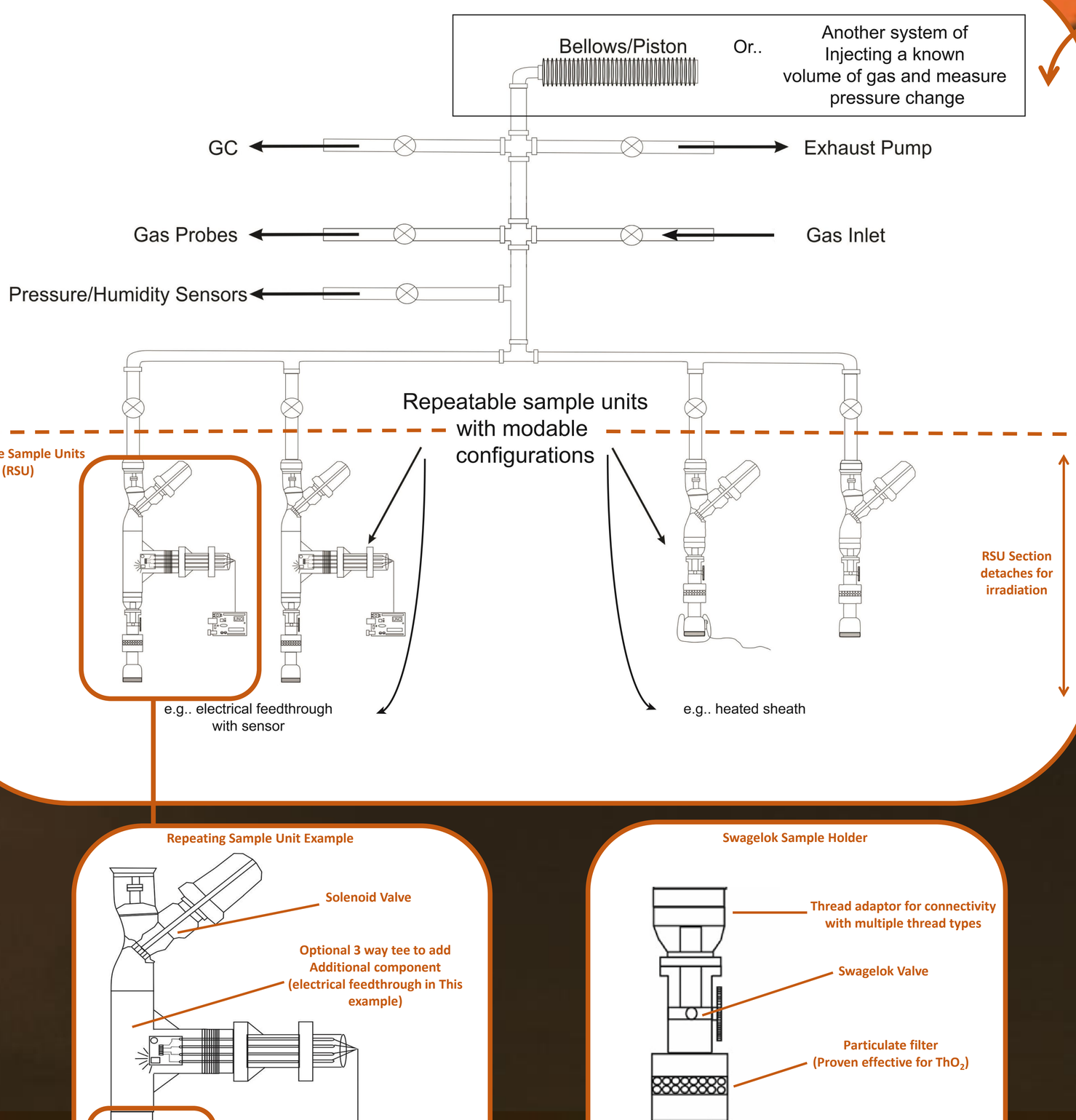

Repeating Sample Unit Example

Swagelok Sample Holder

BME280 RH/T/P Sensor Radiation Hardness test

Wired Sensor monitoring tests

Co^{60} Irradiator Dose Rate for Sensor A & B: ~312Gy/min

Sensor A

- Survival time = <16:15 mins
- Dose for critical damage = 5.03 KGy

Sensor B

- Survival time = <8:32 mins
- Dose for critical damage = 2.59KGy

BME280 RH/T/P Sensor GC testing

H_2 Detection from Gas Chromatography in sealed, argon purged irradiated Sensors (Peak at 1.5)

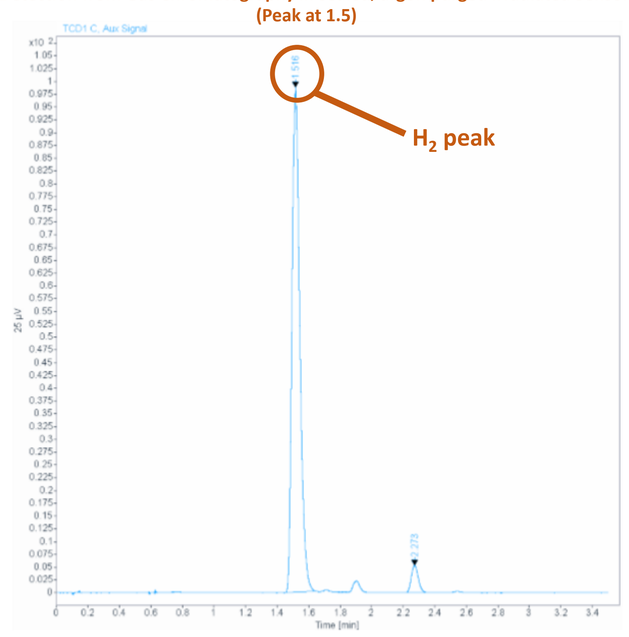

GC Peaks from sealed sensor 1 of 2

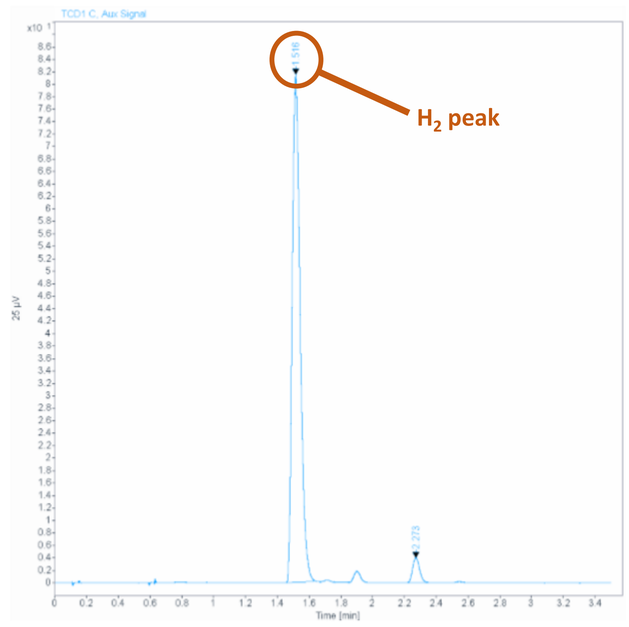

GC Peaks from sealed sensor 2 of 2

*** Detection may be from not-successfully driving off all water although little signs of other gases are present**

Future Planning

The near future will involve the manifold assembly and testing. When successful results are produced with non-active oxides, Uranium oxides and ThO_2 experiments will begin using the previously described apparatus.

Transformative Science and Engineering for Nuclear Decommissioning

Engineering and Physical Sciences Research Council

transcendconsortium.org

Energy For a Low Carbon Future

Atomistic Simulation of PuO_2 Surfaces

Elanor Murray
School of Chemistry, University of Birmingham, B15 2TT
exm350@student.bham.ac.uk

Introduction

The UK has the largest civil stockpile of plutonium in the world, stored at Sellafield. However, ageing mechanisms associated with the storage of PuO_2 are poorly understood [1]. As the PuO_2 is stored in powder form, understanding the surface structures is of high importance. METADISE was used to simulate pure PuO_2 surfaces using interatomic potentials [2]. The relaxed surface energies were compared to determine which surfaces were the most energetically stable and the morphology was predicted.

Pure PuO_2 Surfaces

Pure PuO_2 surfaces were simulated using METADISE. The {*n*10}, {*n*11} and {*nn*1} surfaces were simulated, where *n*=1,2,3. It was found that initially unstable surfaces had a higher percentage relaxation than initially stable surfaces.

The simulations indicate that the {*nn*1} surfaces are the most energetically stable, with {*n*10} surfaces generally being the least stable. The most stable surfaces simulated were: (111), (221) and (331). Fig 2 displays the (111) surface.

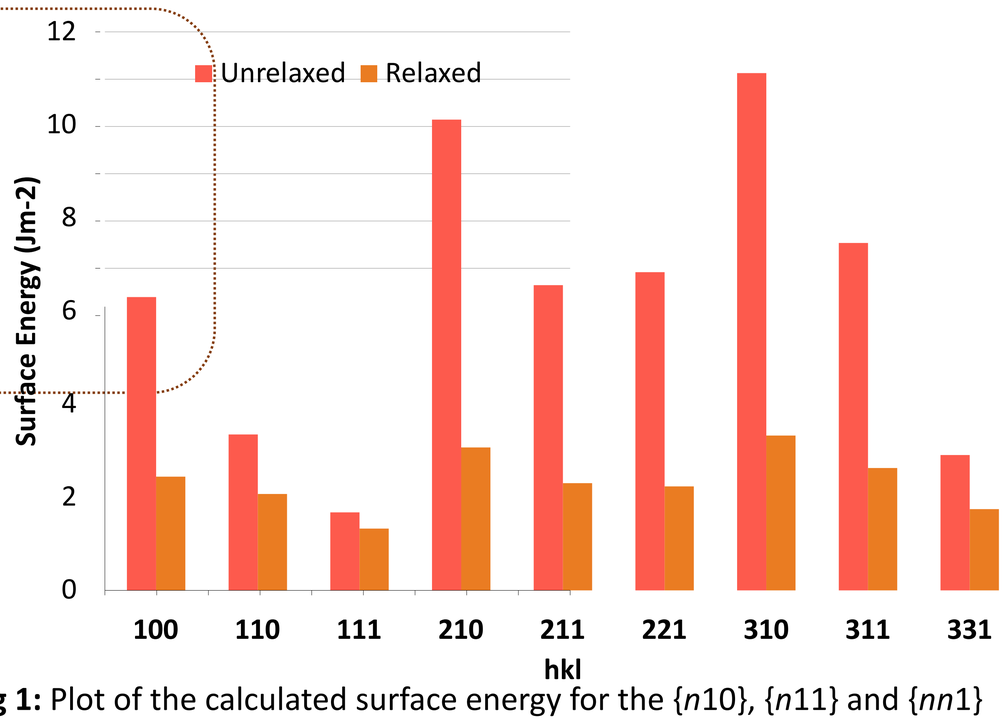

Fig 1: Plot of the calculated surface energy for the {*n*10}, {*n*11} and {*nn*1} surfaces (*n*=1,2,3) before and after the surface was allowed to relax.

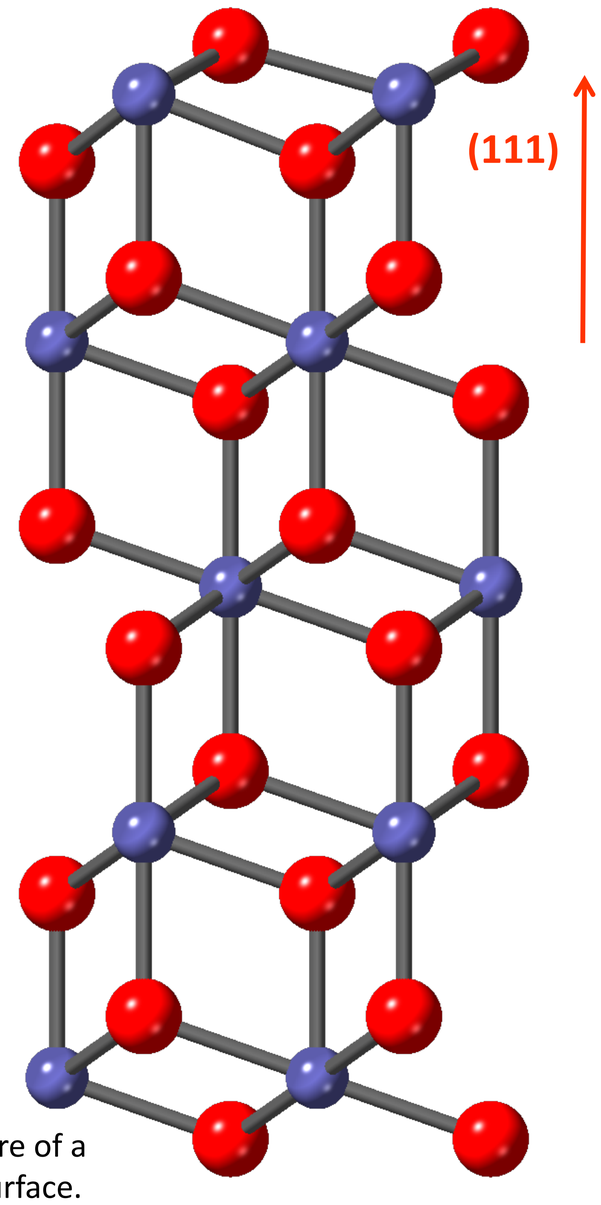

Fig 2: Structure of a (111) PuO_2 surface.

(100) Surface

The {*n*10} surfaces of PuO_2 were found to generally be the least stable. Fig 3 displays the structure of the (100) surface, before and after relaxation. The surface is a Tasker type three surface, consisting of alternating charged layers of O and Pu ions, with a polar surface termination.

In the relaxed structure (RHS Fig 3.) it is evident that the surface has distorted to accommodate the surface dipole. The oxygen layers close to the surface are rumpled and O-Pu separation is reduced. It is possible that the surface may be stabilised by faceting as observed in UO_2 [4].

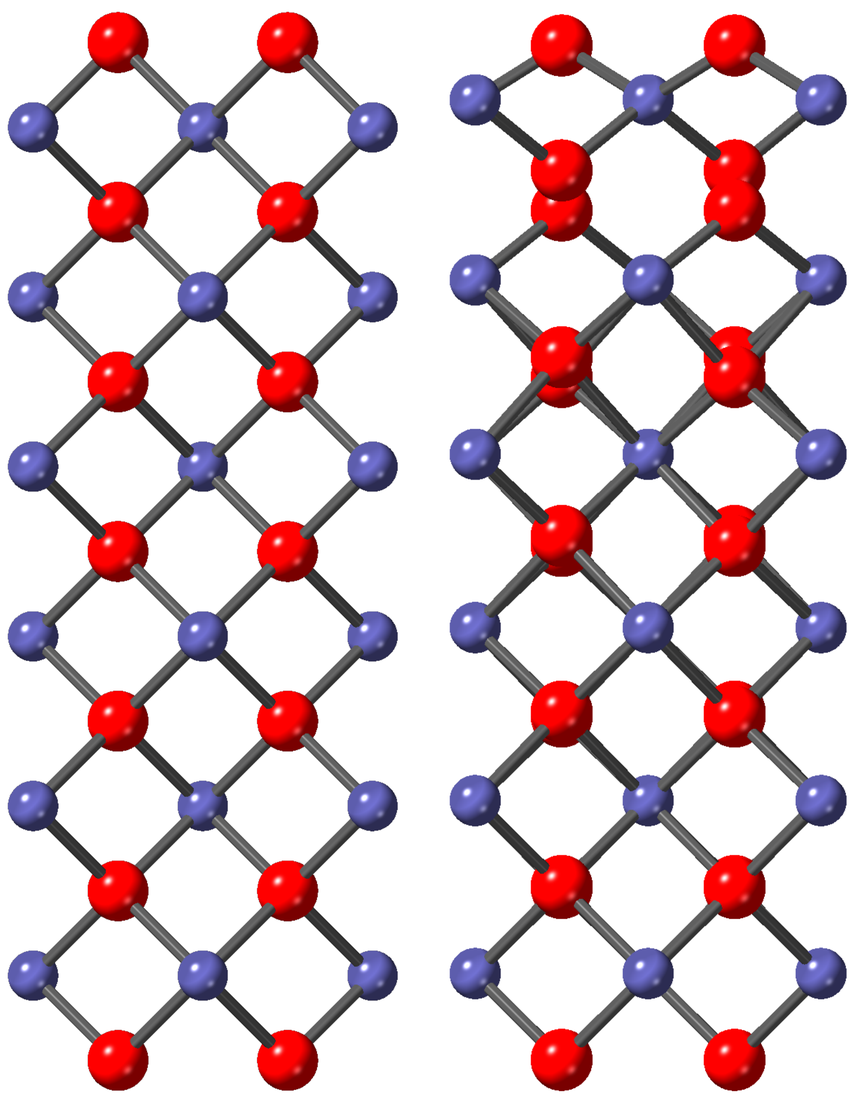

Fig 3: Structure of a (100) PuO_2 surface. LHS before relaxation. RHS after relaxation.

Morph

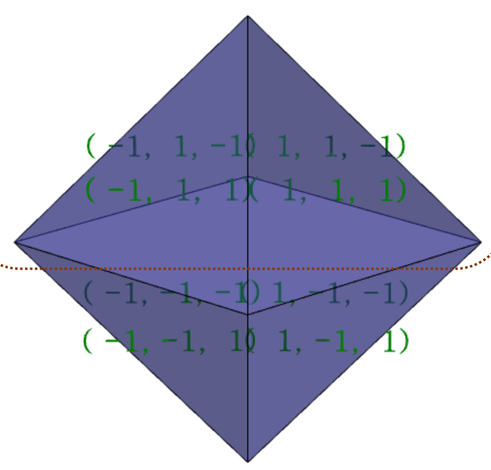

Fig 4: Wulff construction of the equilibrium morphology of PuO_2.

The equilibrium growth morphology of PuO_2 was predicted from the relaxed surface energies, by generation of a Wulff construction (Fig 4.). As can be seen in Fig 4. the crystallite is octahedral shaped. This is due to the (111) surface (Fig 2.) having the lowest energy.

This is in agreement with Wulff constructions of UO_2 [3].

Conclusions and Future Work

- The pure (111) surface was found to be the most energetically stable, in agreement with other binary fluorite structured oxides such as UO_2 [3].
- The next step will be modelling defective surfaces, in order to calculate segregation energies. This will find if there is a thermodynamic drive for defects to migrate from the bulk to the surface.
- Future work will focus on helium incorporation in PuO_2. Key research areas are: how much helium can be accommodated, what are the likely trapping sites and investigating possible mechanisms for helium bubble formation.

References:
[1] Wolfer, W. G. Radiation effects in plutonium. *Los Alamos Sci.* **26**, 274–285 (2000)
[2] Read MSD, Jackson RA. Journal of Nuclear Materials. **406**, 293 (2010)
[3] Abramowski, M.*, et al.*, *Journal of Nuclear Materials* (1999) **275** (1), 12
[4] Taylor, T. N., and Ellis, W. P., *Surface Science* (1978) **77** (2), 321

Acknowledgements:
Dr Mark Read (Supervisor)
Helen Steele (SL), Robin Orr (NNL)
NDA, NNL and EPSRC

A Systematic Investigation of the Zirconolite $CaZr_{1-x}Ce_xTi_2O_7$ Solid Solution as a Potential Wasteform for Plutonium

L.R. Blackburn[a], S.K. Sun[a], L.J. Gardner[a], E.R. Maddrell[b], M.C. Stennett[a], N.C. Hyatt[a]

[a]University of Sheffield, [b]National Nuclear Laboratory

Correspondence: n.c.hyatt@sheffield.ac.uk, shikuan.sun@sheffield.ac.uk

1 Introduction

The United Kingdom is in the process of consolidation all Pu stocks and residues at Sellafield, in order to satisfy proliferation concerns and develop a long term management strategy. The bulk of this inventory is comprised of ~ 120 teHM PuO_2. Immobilisation in a chemically durable ceramic matrix is considered a credible option, producing a stable wasteform compatible with the conditions imposed in the geological disposal environment. The complex oxide zirconolite (nominally $CaZrTi_2O_7$) occurs in many diverse rock types, capable of accommodating significant REE, ACT, Nb, Hf, and is therefore a candidate host phase for the immobilisation of Pu. In the present work, we characterise the phase assemblage and microstructure of the $CaZr_{1-x}Ce_xTi_2O_7$ solid solution, with Ce acting as a structural simulant for Pu [1].

2 Experimental Procedure

All compositions were fabricated by conventional solid state synthesis from mixed oxide precursors. $CaTiO_3$, ZrO_2, TiO_2 and CeO_2 were batched according to $CaZr_{1-x}Ce_xTi_2O_7$ ($0.00 \leq x \leq 0.40$, $\Delta x = 0.10$) and homogenised by ball milling. Specimens were pressed into 10 mm pellets and sintered at 1350 ˚C for 20 h in either air, argon or 5% H_2/N_2.

3 Results and Discussion

Powder X-ray diffraction data for $CaZr_{1-x}Ce_xTi_2O_7$ compositions sintered in air are shown in **Fig. 1**. Single phase zirconolite-2M was obtained for $x \geq 0.10$, with a polymorphic transformation to the zirconolite-4M polytype observed in the interval $0.10 \leq x \leq 0.20$. A minor Ce-bearing perovskite was also present at high Ce concentration (~ 10 wt. % at x = 0.40). The phase evolution under argon and 5% H_2/N_2 was significantly disrupted, with an ancillary perovskite phase occupying a major fraction of the overall assemblage at high Ce content (~ 37 wt. % and ~ 48 wt. %, respectively, corresponding to x = 0.40)

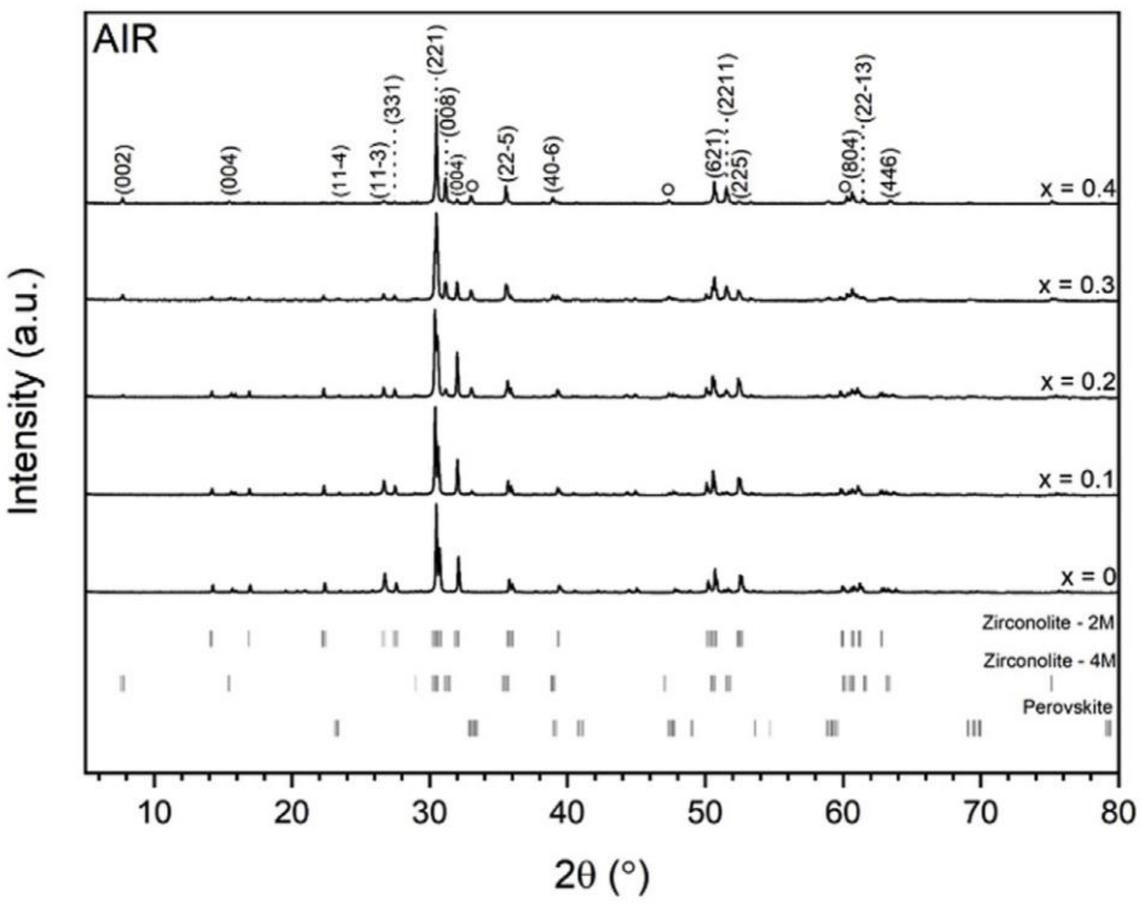

Fig. 1) Powder XRD data for $CaZr_{1-x}Ce_xTi_2O_7$ ($0.00 \leq x \leq 0.40$) compositions sintered in air at 1350 ˚C for 20 h

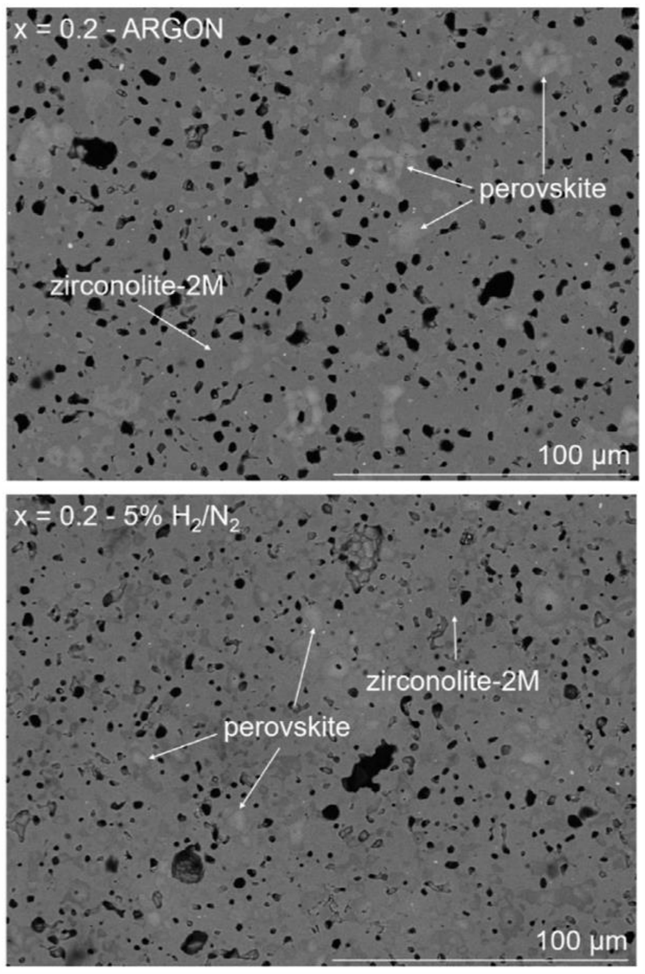

Fig. 2) Representative microstructure for x = 0.20 compositions sintered in argon (top) and 5% H_2/N_2 (bottom)

A representative section of the microstructure corresponding to x = 0.20 for samples sintered in argon and 5% H_2/N_2 is displayed in **Fig. 2**. It was determined from EDS analysis that Ce was preferentially accommodated in a secondary perovskite phase (nominally $CaTiO_3$) at all levels of targeted Ce concentration. It is understood that this may lead to accelerated release of Ce in the disposal environment, due to decreased aqueous durability [2]. It was considered that the sintering environment controlled the phase assemblage *via* Ce valence. Ce L_3 XANES data (**Fig. 3**) demonstrated that Ce^{4+} was the dominant oxidation state during oxidative sintering (however ~ 28% Ce was present as Ce^{3+}). Argon sintering was sufficient to reduce ~ 78% Ce to Ce^{3+}, whilst Ce was uniformly distributed as Ce^{3+} under 5% H_2/N_2. The increase in ionic radii associated with $Ce^{4+} \rightarrow Ce^{3+}$ reduction was considered sufficient to promote preferential accommodation within the Ca^{2+} site of $CaTiO_3$.

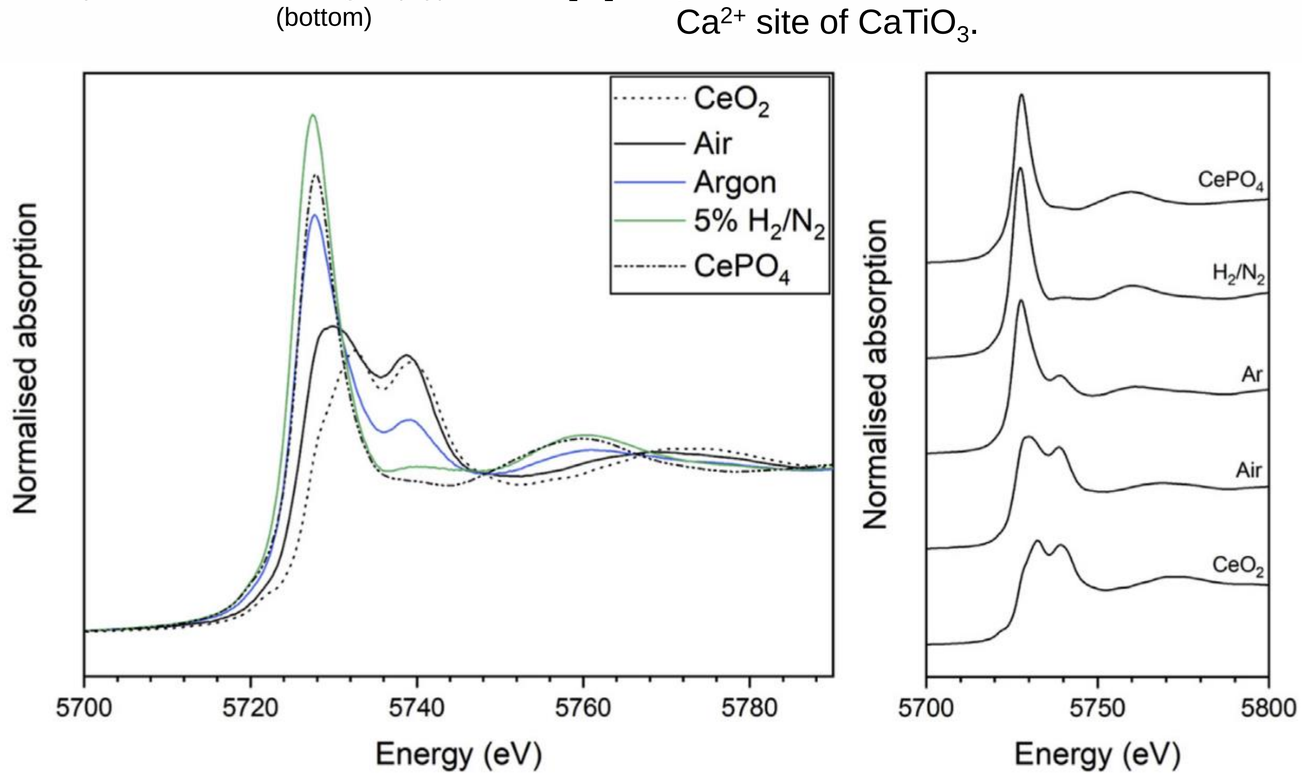

Fig. 3) Ce L_3 XANES spectra corresponding to x = 0.40 composition sintered in air, argon and 5% H_2/N_2, alongside Ce^{3+} and Ce^{4+} reference compounds ($CePO_4$ and CeO_2, respectively).

4 Conclusions

The atmosphere introduced during the sintering of $CaZr_{1-x}Ce_xTi_2O_7$ ceramics was found to influence the resultant phase assemblage by ultimately controlling Ce valence, promoting the formation of a deleterious Ce-perovskite phase under argon and 5% H_2/N_2. This has implications for the corresponding Pu solid solution, by which the most favourable phase assemblage would be expected to form with oxidative sintering, to maintain Pu^{4+}.

References

[1] Blackburn *et al*. J Nucl Mater. 2020; 535

[2] Hyatt *et al*. IOP Conf. Series: Mater. Sci. Eng., 818 (2020)

Acknowledgements

This research utilised the HADES/MIDAS facility at the University of Sheffield established with financial support from EPSRC and BEIS, under grant EP/T011424/1 [2]. We acknowledge EPSRC for funding under grant number EP/S01019X/1.

Chemical durability of Hot Isostatic Pressed Ceramic Materials for the Immobilisation of Stockpiled UK Plutonium

L.R. Blackburn[1], R. Crawford[1], S.A. Walling[1], L.J. Gardner[1], C. Gausse[1], S.K. Sun[1], E.R. Maddrell[2], M.C. Stennett[1], N.C. Hyatt[1] and C.L. Corkhill[1]

[1]: Immobilisation Science Laboratory, Department of Materials Science and Engineering, The University of Sheffield, S1 3JD, UK
[2]: National Nuclear Laboratory, Sellafield, Cumbria, CA20 1PJ, UK

c.gausse@sheffield.ac.uk

Context

- ✓ **~ 140 tons of PuO_2** from UK PUREX reprocessing and AGR fuels
- ✓ UK Nuclear Decommissioning Authority has potential options for reuse or disposal
  - ⇒ Fabrication of **MOX** (Mixed Oxide) Fuels
  - ⇒ **Immobilization** within a chemically durable ceramic matrix

Zirconolite $CaZrTi_2O_7$ and **Hot Isostatic Pressing** (HIP) are candidates for Pu stockpile disposition

- ✓ **Zirconolite-2M**
- ✓ Polymorphic transitions observed with the incorporation of An and Ln
- ✓ Pu can be accepted within Ca^{2+} and Zr^{4+} sites

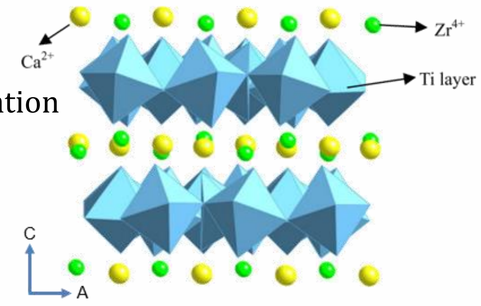

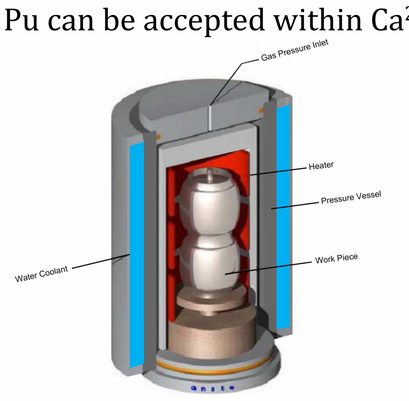

- ✓ Simultaneous pressure and heat through Argon gas
- ✓ **High density** ceramic wasteforms
- ✓ **Large Volume of reduction**
- ✓ **Insensitivity** to physicochemical nature of waste

Synthesis and Characterisation

- ✓ Solid state reaction

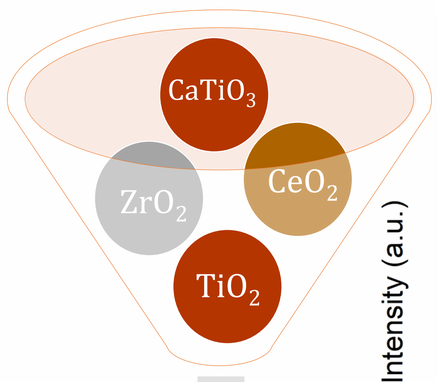

HIPed at 1300°C – Ar

$CaZr_{0.8}Ce_{0.2}Ti_2O_7$

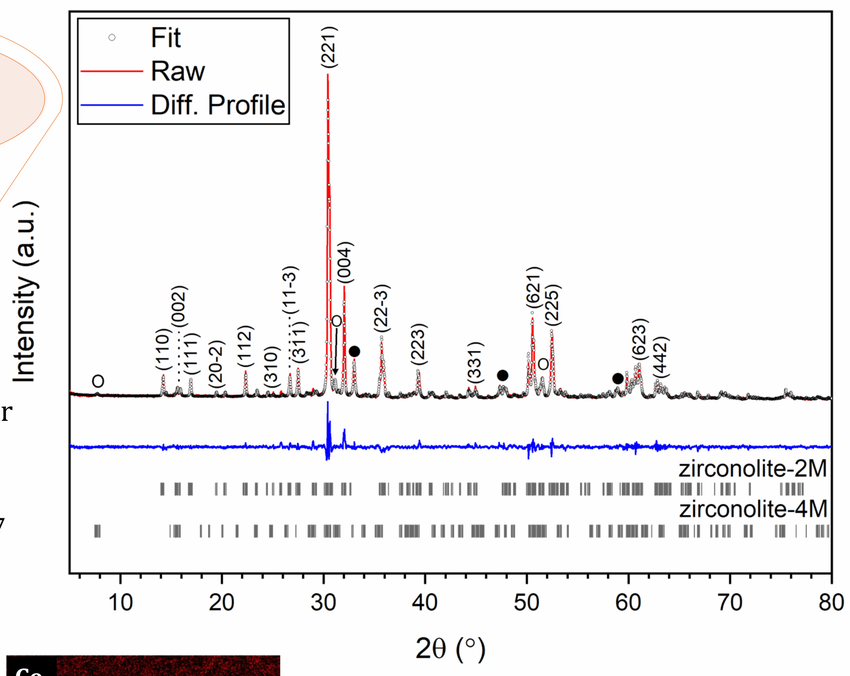

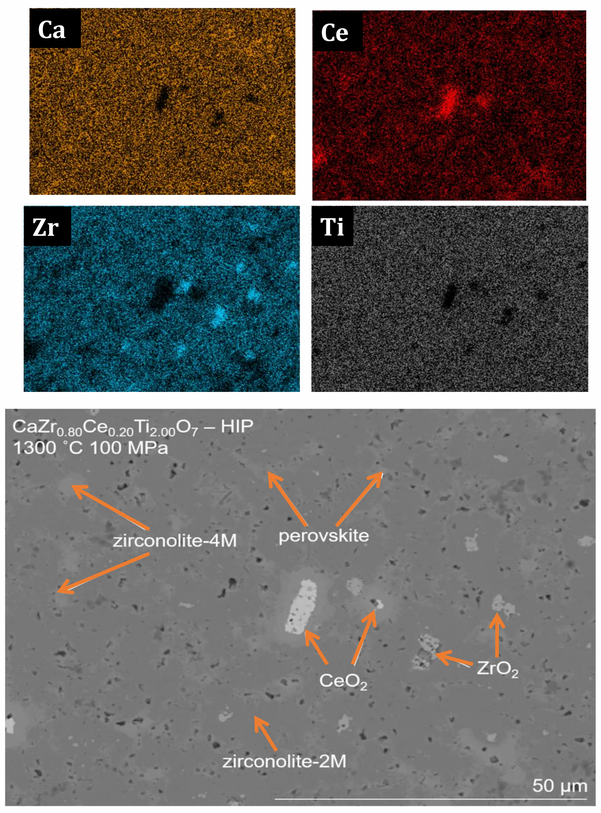

- ✓ Co-existence of Zirconolite-2M and 4M
  - ⇒ Solubility limit of Zirconolite-2M reached
- ✓ Presence of Perovskite ($CaTiO_3$) at 2θ = 33°
  - ⇒ May be detrimental to wasteform durability
- ✓ Minor ZrO_2 and CeO_2
  - ⇒ Incomplete immobilization of Ce within ceramic framework

Chemical durability of Ce surrogate wasteform

- ✓ PCT-B dissolution tests (SA/V = 600 m^{-1})
- ✓ 75–150 µm size fraction
- ✓ Static leaching experiments at 90°C – 7 days

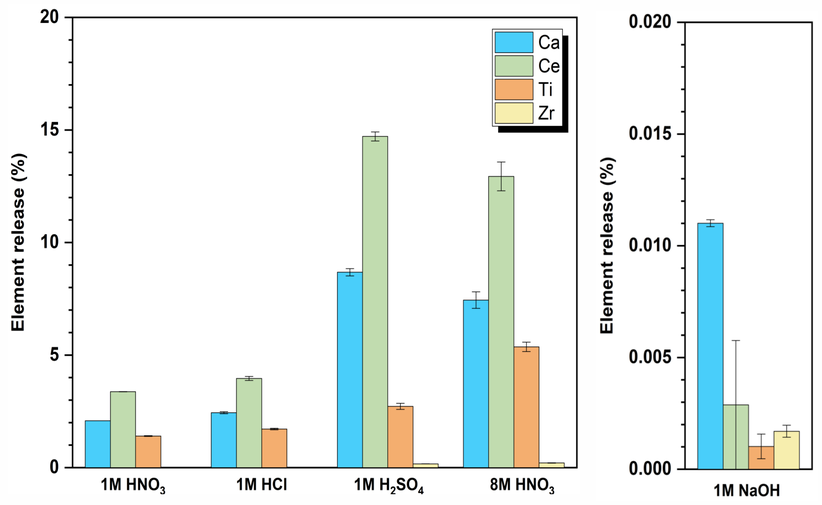

- ✓ Extensive dissolution in 8 M HNO_3 and 1 M H_2SO_4
- ✓ Insignificant dissolution in 1 M NaOH
  - ⇒ Increased wasteform durability in high pH

- ✓ Zirconolite demonstrates excellent chemical durability over e.g. perovskite, hollandite, rutile
- ✓ Co-partitioning of Ce within $CaTiO_3$ responsible for enhanced leaching rates

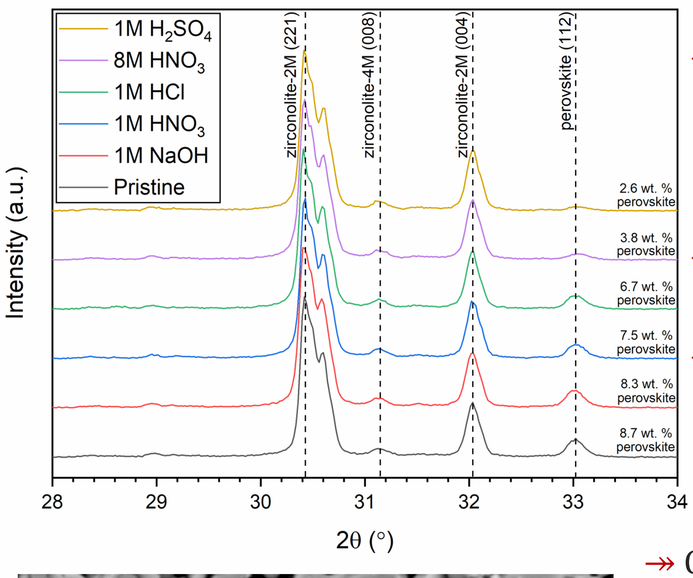

- ✓ Quantity of perovskite relative to zirconolite decreases systematically with observed cerium leaching
- ✓ No variation in zirconolite intensity
- ✓ Ce^{3+} more readily accommodated without charge balance species
  - ⇒ $Ce^{4+} \rightarrow Ce^{3+}$ mechanism proposed due to reduction environment of HIP canister

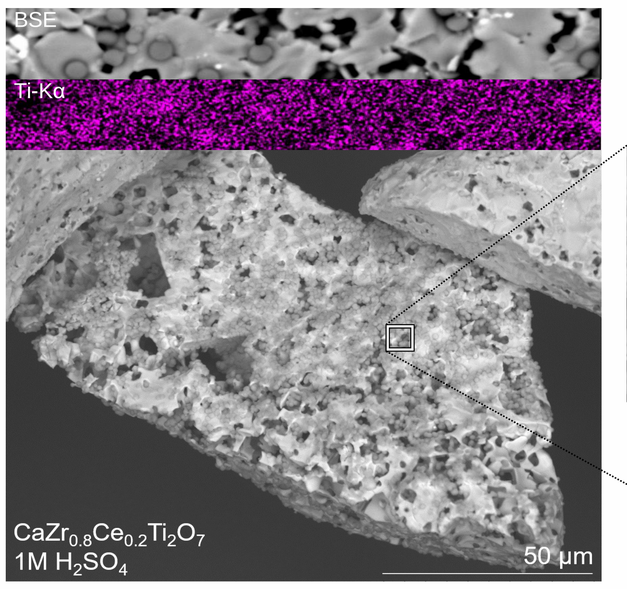

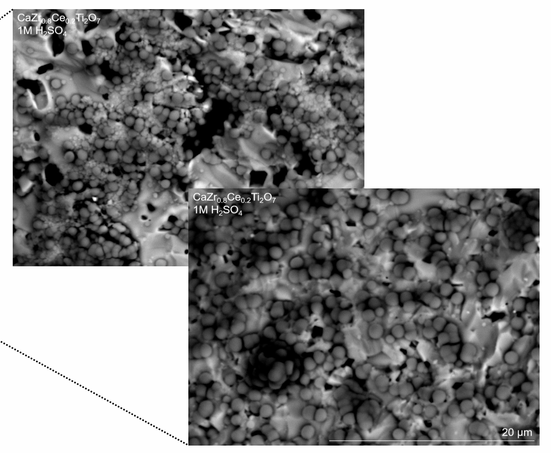

- ✓ Preferential phase dissolution and surface precipitation
  - ⇒ EDS and PHREEQ-C modeling suggest TiO_2 precipitation

Conclusion

- ✓ **High density ceramic wasteforms** for Pu immobilisation thanks to HIP
- ✓ **Pre-processing optimisation** needed to improve microstructural homogeneity
- ✓ HIP environment promotes **$Ce^{4+} \rightarrow Ce^{3+}$ reduction**, and preferential uptake in secondary perovskite phase
- ✓ **Perovskite has lower aqueous durability** with respect to zirconolite, leading to incongruent dissolution of Ce from ceramic wasteform
- ✓ **Promising implications for Pu immobilisation**
- ✓ Further work aims for active validation (U/Th surrogates) and assessment of Pu retrievability from HIP wasteforms

Transformative Science and Engineering for Nuclear Decommissioning

EPSRC UK Research and Innovation | NATIONAL NUCLEAR LABORATORY | NDA Nuclear Decommissioning Authority | The University Of Sheffield. | NucleUS Immobilisation Science Laboratory | Energy For a Low Carbon Future